DNA origami nanoplate-based emulsion with designed nanopore function

Daisuke Ishikawa,[a†] Yuki Suzuki,[b] Chikako Kurokawa,[c] Masayuki Ohara,[d] Misato Tsuchiya,[a] Masamune Morita,[a] Miho Yanagisawa,[c] Masayuki Endo,[e] Ryuji Kawano,[d] Masahiro Takinoue[a*]

[a]*Department of Computational Intelligence and Systems Science, Tokyo Institute of Technology, 4259 Nagatsuta-cho, Midori-ku, Yokohama, Kanagawa 226-8502, Japan*

[b]*Frontier Research Institute for Interdisciplinary Sciences, Tohoku University, 6-3 Aramaki aza Aoba, Aoba-ku, Sendai 980-8578, Japan*

[c]*Department of Applied Physics, Faculty of Engineering, Tokyo University of Agriculture and Technology, 2-24-6 Naka-cho, Koganei, Tokyo 184-8588, Japan*

[d]*Department of Life Science and Biotechnology, Tokyo University of Agriculture and Technology, 2-24-6 Naka-cho, Koganei, Tokyo 184-8588, Japan*

[e]*Department of Chemistry, Graduate School of Science, Kyoto University, Yoshida-ushinomiyacho, Sakyo-ku, Kyoto 606-8501, Japan*

*Correspondence to: M. Takinoue (takinoue@c.titech.ac.jp)

†Present address: Department of Applied Chemistry, Tokyo Metropolitan University, 1-1 Minami-osawa, Hachioji, Tokyo, Japan

Abstract

Bio-inspired functional microcapsules stabilised with surfactants, copolymers, and nano/microparticles have attracted much attention in many fields from physical/chemical science to artificial cell engineering. Although the particle-stabilized microcapsules have advantages for their stability and rich ways for functionalisation such as surface chemical modifications and shape control of particles, versatile methods for their designable functionalisation are desired to expand their possibilities. Here, we report a DNA-based microcapsule composed of a water-in-oil microdroplet stabilised with amphiphilised DNA origami nanoplates. By utilising function programmability achieved by DNA nanotechnology, the DNA nanoplates were designed as a nanopore device for ion transportation as well as the interface stabiliser. Microscopic observations showed that the microcapsule formed by amphiphilic DNA nanoplates accumulated at the oil-water interface. Ion current measurements demonstrated that pores in the nanoplates functioned as ion channels. These findings provide a general strategy for programmable designing of microcapsules for engineering artificial cells and molecular robots.

Introduction

Bio-inspired compartmental microcapsules[1] have attracted much attention as promising chemical microreactors for chemical and biological analysis[2–4], molecular evolution[5,6], nonequilibrium chemical reactions[7–9], drug delivery and artificial exosomes[10], artificial cells[11–16], and cell-like molecular robots[18–21]. The microcapsules are generally produced as vesicles or droplets (emulsions) stabilised with amphiphilic molecules such as surfactants[5,6,8], natural/synthetic lipids[12–17], and copolymers[22]. The chemical reaction capabilities of the microcapsules have often been enhanced by adding biomimetic functions such as environmental responses[22] and substrate exchange[8,12,23,24]. For example, the substance permeability of lipid-bilayer microcapsules, also called liposomes, have been enhanced by adding synthetic lipids with modified permeability[24], and natural membrane channel proteins[12,13]. Recently, the functionalisation of liposomes with DNA nanodevices such as sensors[25] and nanopores[19,26] constructed with DNA motifs[27] or DNA origami[28] has also been challenged, which is a hopeful method thanks to designability and programmability of DNA nanodevices.

Besides amphiphilic molecules, nano/microparticles can also stabilise compartmental microcapsules, which are referred to as colloidosomes[29] for vesicle-type microcapsules and Pickering emulsions[22,30,31] for droplet-type ones. Such particle-stabilised microcapsules have advantages of not only their stability but also the possibility of rich ways for functionalisation. Such particle-stabilised microcapsules are often functionalised by surface modification of particles[32], shape control of amphiphilic particles[33], and utilization of functional materials for the particles[34]. For example, a stimuli-responsive gating of molecules for the colloidosomes was achieved by modifying nanoparticles with a thermosensitive polymer[23]. However, designable and programmable functionalisation of the particle-stabilised microcapsules has not been achieved yet. To receive the full benefit of the particle-stabilised microcapsules, a versatile

method to functionalise the microcapsules is desired.

Here, we report a DNA-based microcapsule (Fig. 1a) composed of a water-in-oil (W/O) microdroplet stabilised with amphiphilised DNA origami nanoplates. The DNA nanoplate work not only as a nanoparticle-based stabiliser of microcapsules but also as a nanodevice functioning in ion transportation (Fig. 1b). The formation mechanism of the microcapsules is expected to be the Pickering-like emulsion rather than the surfactant- or lipid-stabilised emulsions[35,36]. Generally, stabilising particles of Pickering emulsions must be (i) much smaller than the droplet size, (ii) partially wettable to both water and oil phases to adsorb at their interface, and (iii) accumulated on the interface with weak mutual interactions among the particles. Actually, the amphiphilic DNA nanoplates is a planar amphiphilic nanoparticle of ~100 nm in diameter and ~2 nm in thickness, which is quite larger than surfactants/lipids but much smaller than microdroplets. Of course, the DNA nanoplates are programmable in terms of their functions because they can be constructed based on computer-aided design. We believe that this method provides a strategic approach for programmable design and control of particle-stabilised microcapsules in the many applications aforementioned.

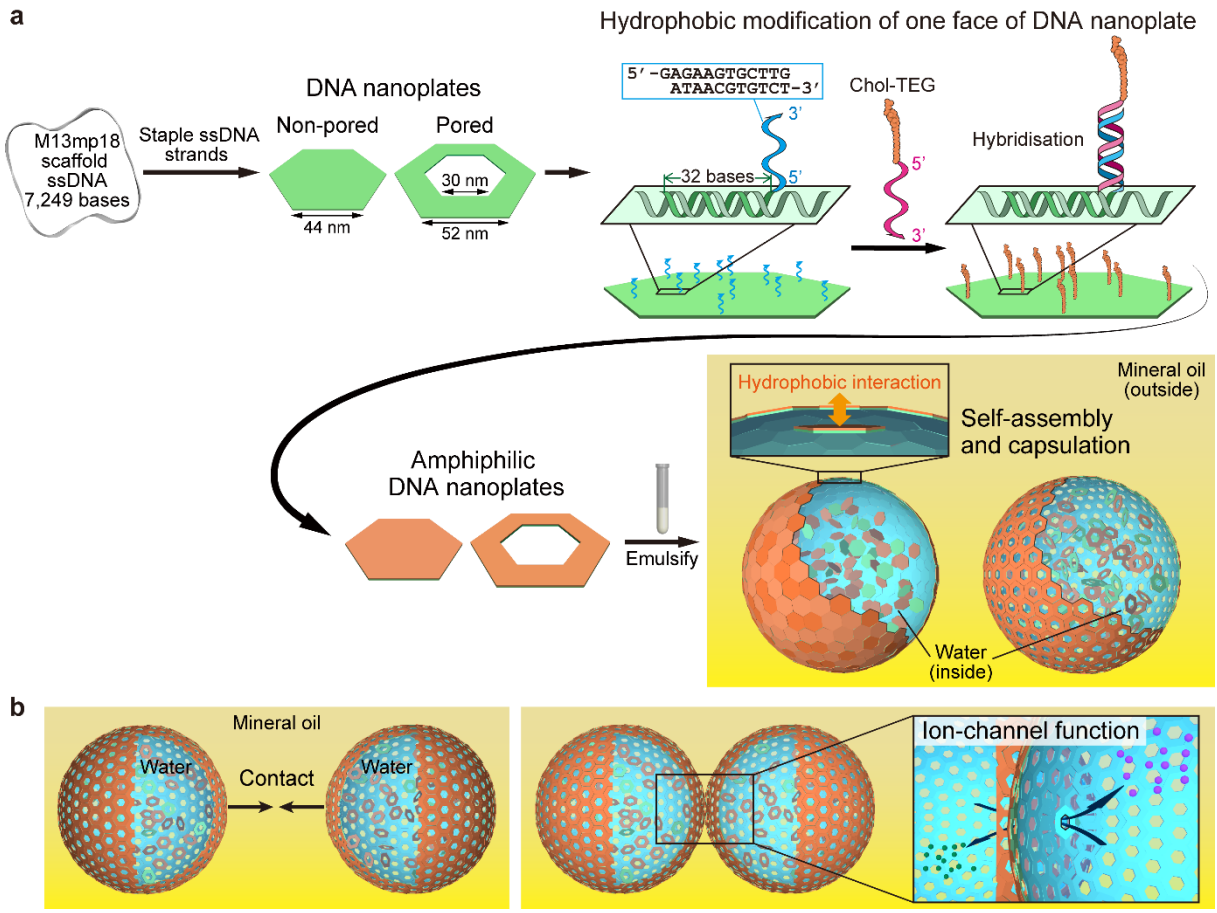

Figure 1. Concept of DNA origami nanoplate-based Pickering emulsion. (a) Schemes for preparation of the amphiphilic DNA nanoplates and its self-assembly at the oil–water interface. Two types of hexagonal DNA nanoplates, without or with a hexagonal pore, are constructed from scaffold ssDNA. Chol-TEG groups as hydrophobic parts to only one face of the nanoplate are selectively introduced after the DNA nanoplate formation. The amphiphilic DNA nanoplates self-assemble at the oil–water interface to form a microcapsule. (b) Functionalisation of the microcapsule with a designed nanopore in the DNA nanoplate. The hexagonal pore can act as an ion channel.

Results and Discussion

Amphiphilic DNA nanoplates. Our approach for microcapsules stabilised with the DNA nanoplates is illustrated in Fig. 1; the nanoplates self-assemble at the oil-water interface and then produce a microcapsule based on a W/O microemulsion. We created two types of nanoplates without and with a pore based on the previous report[37]. The non-pored DNA nanoplate had a hexagonal shape (44 nm each side); the pored DNA nanoplate had a hexagonal shape (52 nm each side) with a centred hexagonal pore (30 nm each side) (Supplementary Fig. 1). Atomic force microscopy (AFM) imaging showed that the designed shapes were accurately formed (Supplementary Fig. 2).

To achieve self-assembly of the DNA nanoplates at an oil-water interface, an amphiphilic property was supplied to the DNA nanoplate by the addition of hydrophobic molecules to only one face of the nanoplate (Fig. 1a); particles of this shape are often referred to as Janus particle[33,38]. Here, the cholesterol-triethyleneglycol group (Chol-TEG) was used as the hydrophobic molecule. First, the Chol-TEG was modified to a single-stranded DNA (ssDNA) tag. Then, the DNA nanoplate was produced using staple DNAs with a tail sequence complementary to the ssDNA tag; all the staple tails were positioned on the same face of the nanoplates by designing the helical phase of DNA in the nanoplate. Finally, the Chol-TEG was conjugated to the designated positions on one face of the nanoplates through hybridisation of the ssDNA tag and the staple tails.

The introduction of Chol-TEGs onto the nanoplates was evaluated. First, AFM imaging demonstrated that the Chol-TEG-modified DNA nanoplates were produced as designed (Figs. 2a and b, and Supplementary Fig. 3). The AFM imaging of Figs. 2a and b was difficult without a surfactant because of the nanoplate aggregation compared to the imaging of Chol-TEG-unmodified DNA nanoplate (Supplementary Fig. 2). We then performed non-denaturing agarose gel electrophoresis of the nanoplates with varying numbers of introduced

Chol-TEGs. In both non-pored and pored DNA nanoplates, the electrophoretic migration of nanoplates decreased as the number of Chol-TEGs increased (Supplementary Fig. 4); little migration was observed particularly when more than 30 Chol-TEGs were introduced. The results of AFM imaging and electrophoresis could be explained by aggregation of Chol-TEG-modified nanoplates caused by the hydrophobic interactions[39,40] Therefore, the DNA nanoplates exhibited sufficient hydrophobicity via the modification of the Chol-TEG.

Microdroplets based on the amphiphilic DNA nanoplates. An aqueous solution of ~7.5 nM amphiphilic non-pored or pored DNA nanoplates with 1× SYBR Gold nucleic acid stain was added to mineral oil, and then W/O microemulsions were produced by hand tapping. Confocal laser-scanning microscopy (CLSM) images of the W/O microemulsions clearly showed that the amphiphilic non-pored and pored DNA nanoplates localised at the oil-water interface, although DNA nanoplates without the Chol-TEGs were homogeneously dispersed in W/O droplets (Figs. 2c and d, Supplementary Fig. 5). Figs. 2e and f show cross-sectional fluorescence intensity profiles of the droplets stabilised with non-pored and pored nanoplates with 24 Chol-TEG, respectively, which show that the amphiphilic DNA nanoplates localised at the interfacial area with a thickness of 6.2% ± 1.5% (mean ± standard deviation) of the radius of the droplets. These results indicated that the amphiphilic nanoplates allowed the formation of W/O microemulsions.

The non-pored DNA nanoplates with 12 or more Chol-TEGs sufficiently localised on the oil-water interface (Fig. 2c), whereas pored DNA nanoplates with even 48 Chol-TEGs less localised (Fig. 2d). To quantitatively evaluate the localisation degree of the nanoplates onto the oil-water interface, we calculated the fluorescence intensity ratio of the droplet interface to its inside (Figs. 2e and f; histograms of Supplementary Figs. 5c and d). The higher the ratio, the more the nanoplates localised on the interface. When the value was lower than 1, the nanoplates

did not localise at the interface but dispersed inside. These results showed that the amphiphilic non-pored DNA nanoplates had higher ratios than the pored DNA nanoplates, indicating that the amphiphilic non-pored DNA nanoplates were easier to localise on the interface than the amphiphilic pored DNA nanoplates. This difference may be explained by the difference in rigidity and wettability of the amphiphilic non-pored and pored DNA nanoplates. More specifically, the centre large pore may result in less rigidity of the pored DNA nanoplate because of its lower density structure, and also may result in its less wettability because of the lower surface density of the Chol-TEGs; these likely caused the pored DNA nanoplates to form more aggregates dispersed in the water phase.

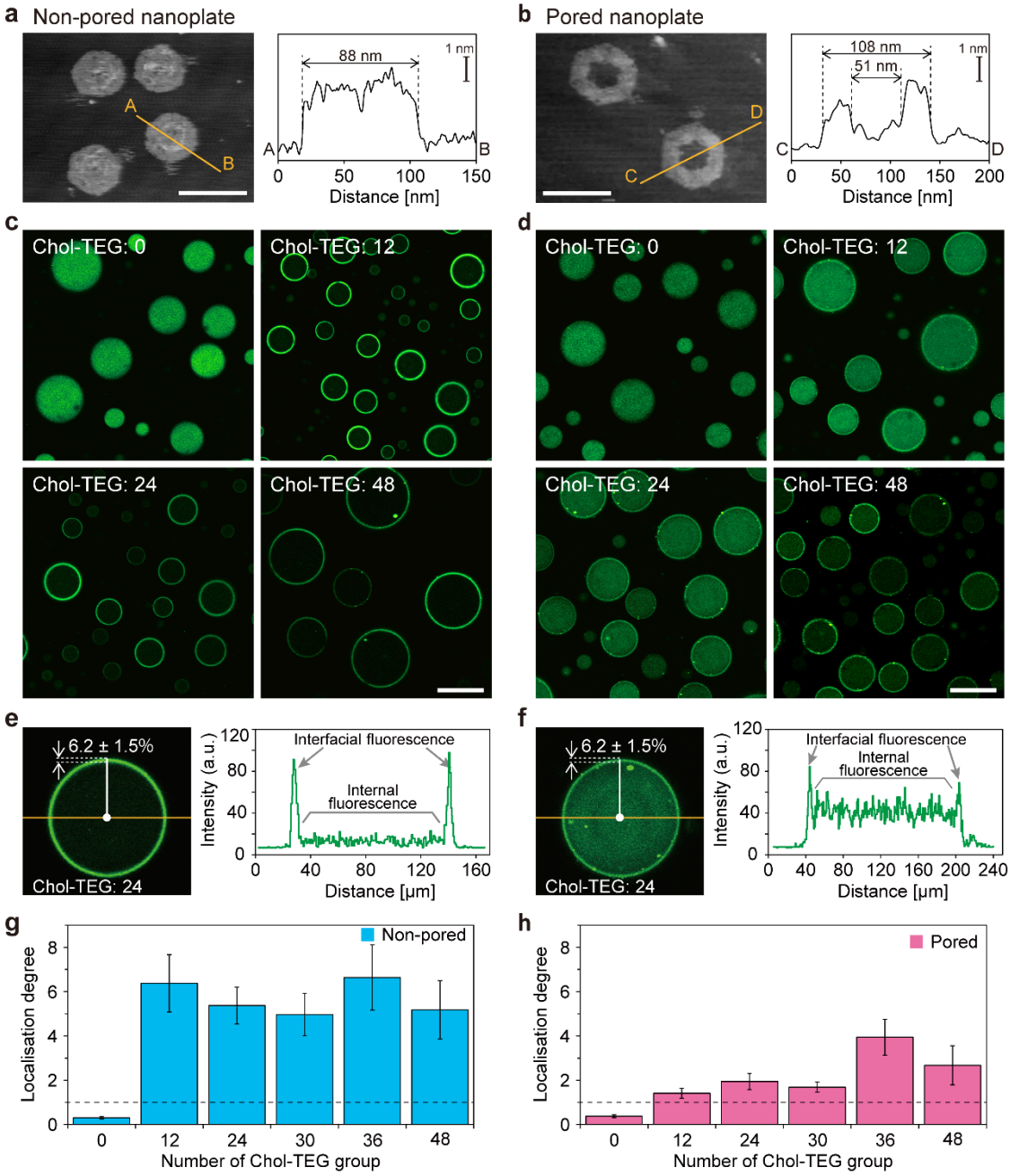

Figure 2. Water-in-oil droplets stabilised with the amphiphilic DNA nanoplates. (a) and (b) AFM images of Chol-TEG-modified non-pored nanoplates (a) and pored nanoplates (b). The cross-sectional profiles were taken along the A–B and C–D lines in the AFM images, respectively. Scale bars: 100 nm. (c) and (d) CLSM images of W/O droplets containing non-pored (c) and pored (d) nanoplates with 0–48 Chol-TEGs. Green fluorescence areas show the location of the DNA nanoplates. Scale bars: 100 μm. (e) and (f) Cross-sectional fluorescence

intensity profiles of the droplets stabilised with amphiphilic non-pored (e) and pored (f) nanoplates with 24 Chol-TEGs. The profiles were measured along the yellow lines. (g) and (h) Localisation degree of (g) non-pored and (h) pored nanoplates modified with 12–48 Chol-TEG groups. The localisation degree was defined as the interfacial fluorescence intensity normalised by the internal fluorescence intensity. The interfacial fluorescence intensity was defined as the average intensity of the interfacial brighter annular area with a thickness of ~6.2% of the droplet radius [shown in (e) and (f)]. The internal fluorescence intensity was defined as the average intensity of the droplet internal area except for the interfacial annular brighter area.

To investigate the state of localisation of the nanoplates, we performed fluorescence recovery after photobleaching (FRAP) of the oil-water interface stabilised with non-pored DNA nanoplates with 24 Chol-TEGs. Here, a fluorophore, 6-carboxyfluorescein group (6-FAM), was conjugated to the nanoplates using the same procedure for Chol-TEG conjugation (Fig. 3a). Fluorescence of the interface of W/O droplets constructed with the fluorescent amphiphilic non-pored DNA nanoplates was recovered to only ~5% after photobleaching (Figs. 3b and c). In contrast, freely diffusing lipids on liposomes or cell membranes are known to generally recover to ~80%[41]. Therefore, lateral diffusion of the amphiphilic nanoplates on the interface was very slow unlike lipids. This result suggests that the nanoplates not only localise on the oil-water interface by amphiphilic adsorption but also partly accumulate by hydrophobic interaction with each other based on partial overlap of the amphiphilic nanoplates[38].

To evaluate how the accumulated amphiphilic nanoplates affected droplet stabilisation, interfacial tensiometry of the W/O droplets was performed. The interfacial tensions of W/O droplets based on the non-pored DNA nanoplates with 0, 12, and 48 Chol-TEGs were 28.8 ± 0.3, 28.2 ± 0.3, and 26.1 ± 0.5 mN m^{-1}, respectively; those based on the pored DNA nanoplates were 28.1 ± 0.1, 27.1 ± 0.1, and 26.1 ± 0.2 mN m^{-1}, respectively. The presence or absence of the centre pore of the DNA nanoplate did not significantly affect the interfacial tension, but the interfacial tensions tended to slightly decrease with the number of Chol-TEGs for both nanoplates. These interfacial tensions were much higher than those of well-known lipids, such as 1,2-dioleoyl-sn-glycero-3-phosphoethanolamine (DOPE) or 1,2-dioleoyl-sn-glycero-3-phosphocholine (DOPC)[42] (about 5.3 and 0.5 mN m^{-1}, respectively). These results suggest that the accumulation of the nanoplates at the oil-water interface did not so strongly contribute to the reduction of interfacial tension but the accumulation involving hydrophobic interaction between nanoplates contributed to preventing the unintended droplet

coalescence. These results are reasonable if the DNA-nanoplate-stabilised droplet was a Pickering-like emulsion as expected because stabilising particles of Pickering emulsions generally interact with each other to form a weakly flocculated state[35,36].

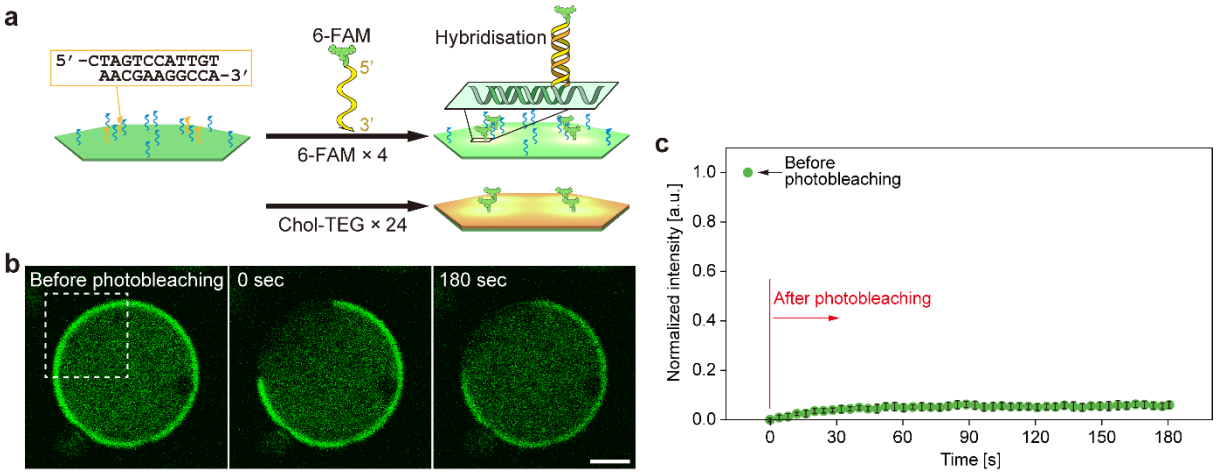

Figure 3. FRAP analysis of the droplet interface to investigate the diffusion of localised DNA nanoplates. (a) Schematic representation for preparing 6-FAM-labelled amphiphilic DNA nanoplate. (b) FRAP analysis for W/O droplet stabilised with 6-FAM-labelled amphiphilic non-pored DNA nanoplate (Chol-TEG: 24). The broken-lined square area was photobleached. Scale bar: 100 μm. (c) Time course of the fluorescence recovery in the photobleaching area, which was normalised by the initial fluorescence intensity before photobleaching.

Ion transport between DNA-nanoplate-based microcapsules. We designed pored DNA nanoplates as ion channels as well as a droplet stabiliser to demonstrate the functionalisation of DNA-nanoplate-based microcapsules. When the centre nanopores of the nanoplates on the contacting surface of two W/O droplets overlap, ions in one droplet are expected to be transferred to the other droplet. Here, the ion channel function of the pored DNA nanoplate with 24 Chol-TEGs was investigated by measuring ion currents using a microchamber device for the droplet contact method[43,44] (Figs. 4a and b). The droplet contact method is often used for measuring ion currents through nanopore proteins on a lipid bilayer membrane.

Figures 4c–e show the current-time traces between the two contacted W/O droplets. When the pored DNA nanoplates were used for both the contacted droplets, step-like current signals were observed (Fig. 4c and Supplementary Fig. 6); in contrast, no current signals were observed when the non-pored DNA nanoplates were used for at least one of the contacted droplets (Figs. 4d and e). Thus, the pored DNA nanoplates allowed the ions to pass through the overlapped nanopores, resulting in step-like current signals commonly observed in ion channel measurements[20,43,44].

Next, we estimated the effective pore size of nanochannels formed by the pored DNA nanoplates on the droplet surfaces. By assuming that one step-like current signal corresponds to one event of nanochannel opening[20,43,44], the effective pore size can be estimated from the following Hille equation[45]:

$$R = \left(l + \frac{\pi r}{2}\right)\frac{\rho}{\pi r^2}, \quad (1)$$

where r and l are the effective pore radius and the channel length of a formed nanochannel, respectively; ρ (~0.171 Ωm) is the electrical resistivity of the buffer solution; and R is the electrical resistance of the pore. R is calculated as $V/\Delta I$ from one step-like signal, where V is the applied constant voltage between the two chambers, and ΔI is the current increase caused by the opening of the single nanochannel.

By assuming that the nanochannel was formed by the contact of two pored DNA nanoplates that were respectively on each contacted droplet interface, $l = 2a$, where a is the thickness of a double stranded DNA (dsDNA) (a~2 nm) (Fig. 4f). Under this assumption, we obtained the distribution of pore diameters of the nanochannel ($2r$) (Fig. 4g, orange). Additionally, the pore diameter of the nanochannel was numerically estimated (Fig. 4g, cyan) based on Monte Carlo simulations for random overlapping of the centre pores of two pored DNA nanoplates (Supplementary Figs. 7a and b). The experimental results showed that the pore diameter $2r$ was 5.6 ± 6.4 nm (average ± standard deviation), whereas the numerically obtained distribution of $2r$ was much larger than the experimental result to be 39 ± 11 nm. We estimated that the actual nanochannel is formed by stacking multiple nanoplates and that the obtained channel diameter $2r$ is considerably smaller than the channel diameter caused by overlapping of a set of nanoplates.

To testify this idea, we assumed that the nanochannel was formed by the contact of N pored DNA nanoplates (N: natural number) on each contacting droplet interface (Fig. 4h); thus, $l = 2Na$. We carried out numerical simulations for $N = 2$–10 (Supplementary Fig. 7c). Figure 4i shows the distribution of pore diameters when $N = 2$; the experimental and numerical distributions did not agree with each other, suggesting that $N \neq 2$. Figure 4j shows the distributions of pore diameters when $N = 7$. In this case, the major peak of the experimental distribution (less than ~20 nm in diameter, including more than 85% of total frequency) almost agreed with the numerical distribution, although the minor peak (~26 nm) was not similar. In addition, Figure 4k shows the distribution of pore diameters when $N = 10$, which also suggests that $N \neq 10$ because of the disagreement between the experimental and numerical distributions. Thus, the nanochannel pore diameter of 4–10 nm was probably produced by statistically ~7-layered random accumulation of the DNA nanoplate pore (~60 nm); meanwhile, the minor peak (~26 nm) may suggest that larger pores sometimes opened where the accumulation layer (N)

was less.

To further investigate the similarity of the major peak of the experimental distribution with that of the numerical distribution, p values of χ^2 tests and Mann-Whitney tests were calculated. As a result, when the significance level was set to 1% in χ^2 test, $p < 0.01$ for Figs. 4g, i and j and $p > 0.01$ for Fig. 4k. Supplementary Table 1 shows the p values of χ^2 tests and Mann-Whitney tests for each N (= 1, 2, …, 10), and the comparison of distributions is shown in Supplementary Fig. 8. These results suggested that $N = 7$ was statistically adequate.

Moreover, when ~7.5 nM of the pored DNA nanoplate was contained in a W/O droplet of ~3.4 mm in diameter (~20 μL in volume) in the microchamber device, approximately 18 layers of nanoplates should be accumulated on the droplet interface under the assumption that all nanoplates were used for accumulation. Because not all the pored DNA nanoplate with 24 Chol-TEGs accumulated on the droplet interface (Figs. 2f and h), the numerical estimation of $N = 7$ will be experimentally reasonable. In addition, the explanation by the multiple-layered accumulation is consistent with the restricted diffusion of nanoplates on the droplet interface as shown in the FRAP experiments (Fig. 3).

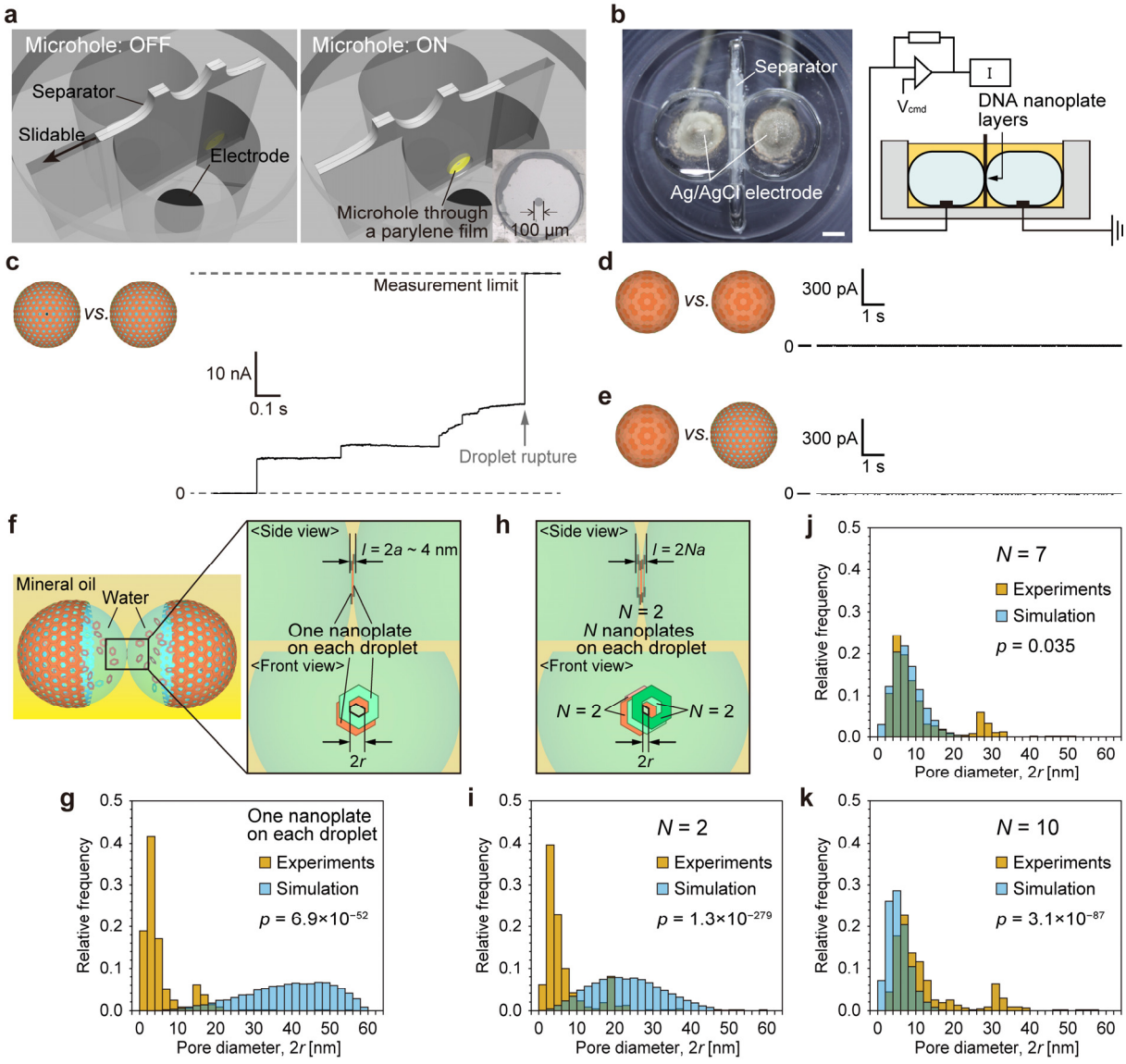

Figure 4. Channel current measurement by the droplet contact method. (a) Schematic illustration of the microdevice. Two chambers are divided by a separator with 100 μm-diameter single hole. (b) The electrodes were at the bottom of the chambers and connected to a patch-clamp amplifier. Scale bar: 1 mm. (c)-(e) Representative current–time traces when (c) both the two droplets were stabilised with pored nanoplates, (d) both were stabilised with non-pored ones, and (e) one was stabilised with non-pored one and the other was stabilised with pored one. The upper limit: ~50 nA. (f) Schematics of the formation of a nanochannel by two DNA nanoplate pores. One nanoplate is on each droplet. The diameter and length of the nanochannel are $2r$ and l=$2a$, respectively. (g) Distributions of $2r$ from experiments and Monte Carlo

simulations when assuming the configuration of (f). (h) Schematics of the formation of a nanochannel by 2N DNA nanoplate pores (N nanoplates on each droplet). The diameter and length of the nanochannel are 2r and l=2Na, respectively. (i)-(k) Distributions of 2r from experiments and simulations when assuming the configuration of (h), where (i) N = 2, (j) N = 7, (k) N = 10.

Conclusions

We demonstrated W/O droplet-based microcapsules constructed with amphiphilic DNA nanoplates. Using pored DNA nanoplates, ion channels between two W/O droplets were achieved; the DNA nanopores successfully worked as nanochannels even though multiple pored DNA nanoplates accumulated on the W/O interface. This successfully demonstrates the integration of a designed and programmable function (here, nanochannel) into interface-stabilising particles of Pickering-like emulsion. Based on this technology, the nanochannel could be improved to a stimuli-responsive gate by the integration of stimuli-responsive conformational change of DNA into the pored DNA nanoplates[23,25] in the future.

FRAP analysis, ion channel current measurement, and pore diameter evaluation suggested that the DNA nanoplates on the W/O droplet interface formed a multi-layered structure with very slow diffusion. The structure probably increased the rigidity of the droplet surface and prevented coalescence between droplets. Therefore, to design the functions of the DNA nanoplate-stabilised microdroplets, the multi-layered accumulation of nanoplates may be required in this method. Meanwhile, microdroplet stabilised with a monolayered DNA nanoplates may be achieved by changing the shape of nanoplates or the amphiphilisation pattern on the nanoplate surface.

In conclusion, our amphiphilic DNA nanoplate-based microcapsules may facilitate the development of multifunctional microcapsules for various applications, such as drug delivery and molecular robots. In particular, colloidosome-like microcapsules constructed with our amphiphilic DNA nanoplates may be useful for such applications. If a microcapsule based on amphiphilic DNA nanoplates with DNA sensors[25] and DNA actuators[46] is integrated with autonomous DNA computers[47,48] into the microcapsule, dynamically and autonomously acting molecular robots[18] may be obtained in the future. Using this system, such DNA nanodevices with novel functions will be “installed like a software” onto the DNA nanoplate-based interface

as an “operating system”.

Methods

Chemicals and reagents used in this study are described in Supplementary Method 1.

Design of DNA nanoplates

Non-pored and pored DNA nanoplates were designed using the square-lattice version of caDNAno software[49] (Supplementary Figs. 1, 9, and 10; Supplementary Tables 2 and 3). As the scaffold strand, the 7,249-nucleotide (nt) long M13mp18 single strand was chosen. Of the 7,249 nt, 6,484 and 6,480 nt were incorporated into each non-pored DNA nanoplate and pored DNA nanoplate with the help of 195 and 216 staple strands, respectively.

For introduction of the Chol-TEG and the 6-FAM into the DNA nanoplates, ssDNAs with 23-nt long orthonormal sequences[50] were used. The orthonormal sequences had low probability of mis-hybridisation and unintended self-folding. For the use of Chol-TEG and 6-FAM labelling, we selected two optimal orthonormal sequences from 37 candidate sequences previously reported[50] through thermodynamic estimations using the Nucleic Acid Package (NUPACK; http://www.nupack.org/) (Supplementary Method 2, Supplementary Figs. 11–13, Supplementary Table 4,).

Preparation and investigation of amphiphilic DNA nanoplates

Non-pored and pored DNA nanoplates were prepared as follows. First, a mixture of M13mp18 ssDNA and staple strands was brought to 50 μL using buffer solution containing 20 mM Tris-HCl (pH 8.0), 1.0 mM EDTA (pH 8.0), and 10 mM $MgCl_2$. The final concentration of M13mp18 ssDNA in the solution was 10 nM, and the molar ratio of the scaffold ssDNA to all the other staple strands was 1:8. The mixture was annealed by reducing the temperature from

85 to 15°C at a rate of –0.1 °C/min in a thermocycler (BM Equipment Co., Ltd., Japan). The nanoplate solution was purified using a Sephacryl S-300 gel-filtration column after annealing. The Chol-TEG-modified ssDNA with the chosen orthonormal sequence of 23 bases (~10 equiv.) was added to the purified sample, followed by incubation at room temperature for 4 h. The Chol-TEG-modified nanoplate was further purified using a gel-filtration column. When 6-FAM-labelled amphiphilic non-pored DNA nanoplates were prepared for FRAP analysis, 6-FAM-labelled ssDNA with another orthonormal sequence (> 10 equiv.) was added to the first purified sample, followed by modification with Chol-TEGs.

The constructed DNA nanoplates were investigated based on AFM imaging (high-speed AFM system; BIXAM, Olympus, Tokyo, Japan) and non-denaturing agarose gel electrophoresis, whose detailed methods are described in Supplementary Methods 3 and 4, respectively.

Investigation of DNA nanoplate-stabilised microdroplets

The microscopic observations and the FRAP analysis were performed using a CLSM (FV1000; Olympus). A 473-nm diode laser was used for fluorescence excitation. The detailed methods are described in Supplementary Method 5.

Interfacial tensions of microdroplets containing the non-pored and pored nanoplates in mineral oil were measured using a contact angle meter (DM-501; Kyowa Interface Science Co., Japan). The interfacial tensions were measured by the pendant drop method based on Young-Laplace fitting. The detailed methods are described in Supplementary Method 6.

Measurement of ion current between droplets

Electrophysiological measurements were performed with the droplet contact method[42–44] using a fabricated microdevice. The microdevice design and fabrication is shown in Supplementary

Method 7. The channel current was monitored using a Pico patch-clamp amplifier (Tecella, Foothill Ranch, CA, USA). The droplet contact method was performed by adding mineral oil (4 μL) and sample solution (20 μL) containing 7.5 nM pored/non-pored DNA nanoplates amphiphilised with 24 Chol-TEGs, 0.5 M KCl, 5 mM Tris-HCl (pH 8.0), 0.25 mM EDTA (pH 8.0), and 2.5 mM $MgCl_2$ to each chamber in order. A constant voltage of +100 mV was applied from the recording side. The measurements started when the separator was set to the "Open" condition (Fig. 4a, right) after sufficient relaxation time of Brownian motion-based accumulation of nanoplates onto the droplet interface by setting the microhole to the "Closed" condition (Fig. 4a, left). The channel current signals were analysed using pCLAMP ver. 10.6 (Molecular Devices, Sunnyvale, CA, USA). The detailed methods are described in Supplementary Method 7.

Production of pore distributions by Monte Carlo simulations

The simulation method is illustrated in Supplementary Fig. 7. The centre nanopore of the DNA nanoplate is assumed to be a circle with a radius r (= 30 nm). $2N$ circles are stochastically placed in a large circle with a radius $2r$. The overlapped area (S) of all of $2N$ circles is the through-hole between the two droplets produced by centre pores of the $2N$ DNA nanoplates. The nanochannel diameter ($2r$) is calculated from $2r = 2\sqrt{S/\pi}$. From 10000 Monte Carlo simulations, the diameter distributions were obtained. Numerical simulations were performed using MATLAB (MathWorks, MA, USA). The statistical analysis used to compare the numerical results with the experimental results was performed using Mathematica (Wolfram Research, IL, USA).

Acknowledgements

We thank Dr. Yusuke Sato (Tokyo Tech) for helpful discussions. This work was supported by a Grant-in-Aid for Scientific Research on Innovative Areas "Molecular Robotics" to M.

Takinoue (M.Tk.) (No. 24104002) and R. K. (No. 15H00803) from The Ministry of Education, Culture, Sports, Science, and Technology (MEXT); a Grant-in-Aid for Scientific Research (B) to M.Tk. (No. 26280097, 17H01813), R.K. (No. 17H01813) and M.E. (No. 15H03837), Challenging Research (Exploratory) to M.Tk. (No. 18K19834) and Y.S. (No. 18K19831) and Grant-in-Aid for Challenging Exploratory Research to M.E. (No. 16K14033) from the Japan Society for the Promotion of Science (JSPS); Research Encouragement Grants from The Asahi Glass Foundation to M.Tk. and D.I.; and Foundation from Oil & Fat Industry Kaikan to D.I; Research grants from The Naito Foundation to M.Y.

Author contributions

M.Tk. conceived the original idea. D.I. primarily contributed to the production of experimental results. D.I. and M.Tk. wrote the manuscript, and all authors revised the manuscript. Y.S. performed the AFM imaging. C.K. and M.Y. measured the interfacial tension. M.O. and R.K. designed and prepared the microdevice for the droplet contact method. M.Tk. and M. Tsuchiya performed the Monte Carlo simulation. M.M. aided in data interpretation. M.E. provided direction for the design of the nanoplates. All authors have agreed to all the content of the manuscript.

Competing financial interests

The authors declare no competing financial interests.

References

1. Schoonen, L. & van Hest, J. C. M. Compartmentalization approaches in soft matter science: from nanoreactor development to organelle mimics. *Adv. Mater.* **28**, 1109–1128 (2016).
2. Griffiths, A. D. & Tawfik, D. S. Miniaturising the laboratory in emulsion droplets. *Trends*

Biotechnol. **24**, 395–402 (2006).

3. Guo, M. T., Rotem, A., Heyman, J. A. & Weitz, D. A. Droplet microfluidics for high-throughput biological assays. *Lab Chip* **12**, 2146 (2012).
4. Kawano, R. *et al.* Rapid detection of a cocaine-binding aptamer using biological nanopores on a chip. *J. Am. Chem. Soc.* **133**, 8474-8477 (2011).
5. Tawfik, D. S. & Griffiths, A. D. Man-made cell-like compartments for molecular evolution. *Nat. Biotechnol.* **16**, 652–656 (1998).
6. Ichihashi, N. *et al.* Darwinian evolution in a translation-coupled RNA replication system within a cell-like compartment. *Nat. Commun.* **4**, 1–7 (2013).
7. Weitz, M. *et al.* Diversity in the dynamical behaviour of a compartmentalized programmable biochemical oscillator. *Nat. Chem.* 6, 295–302 (2014).
8. Sugiura, H. *et al.* Pulse-density modulation control of chemical oscillation far from equilibrium in a droplet open-reactor system. *Nat. Commun.* **7** (2016).
9. Genot, A. J. *et al.* High-resolution mapping of bifurcations in nonlinear biochemical circuits. *Nat. Chem.* **8**, 760–767 (2016).
10. Garcia-Manrique, P., Gutierrez, G. & Blanco-Lopez, M. C. Fully artificial exosomes: Towards new theranostic biomaterials. *Trends. Biotechnol.* **36**, 10–14 (2018).
11. Takinoue, M. & Takeuchi, S. Droplet microfluidics for the study of artificial cells. *Anal. Bioanal. Chem.* **400**, 1705–1716 (2011).
12. Noireaux, V. & Libchaber, A. A vesicle bioreactor as a step toward an artificial cell assembly. *Proc. Natl. Acad. Sci. U. S. A.* **101**, 17669–17674 (2004).
13. Villar, G., Graham, A. D. & Bayley, H. A tissue-like printed material. *Science* **340**, 48–52 (2013).
14. Elani, Y., Law, R. V. & Ces, O. Vesicle-based artificial cells as chemical microreactors with spatially segregated reaction pathways. *Nat. Commun.* **5** (2014).

15. Kurihara, K. *et al.* Self-reproduction of supramolecular giant vesicles combined with the amplification of encapsulated DNA. *Nat. Chem.* **3**, 775–781 (2011).
16. Kurokawa, C. *et al.* DNA cytoskeleton for stabilizing artificial cells. *Proc. Natl. Acad. Sci. U. S. A.* **114**, 7228–7233 (2017).
17. Kunitake T. Synthetic Bilayer-Membranes - Molecular Design, Self-Organization, and Application. *Angew. Chem. Int. Ed.* **31**, 709–726 (1992).
18. Hagiya, M., Konagaya, A., Kobayashi, S., Saito, H. & Murata, S. Molecular Robots with Sensors and Intelligence. *Acc. Chem. Res.* **47**, 1681–1690 (2014).
19. Sato, Y., Hiratsuka, Y., Kawamata, I., Murata, S. & Nomura, S. M. Micrometer-sized molecular robot changes its shape in response to signal molecules. *Sci. Robot.* **2**, eaal3735 (2017).
20. Langecker, M. *et al.* Synthetic Lipid Membrane Channels Formed by Designed DNA Nanostructures. *Science* **338**, 932–936 (2012).
21. Keber, F. C. *et al.* Topology and dynamics of active nematic vesicles. *Science* **345**, 1135–1139 (2014).
22. Meng, F. H., Zhong, Z. Y. & Feijen, J. Stimuli-Responsive Polymersomes for Programmed Drug Delivery. *Biomacromolecules* **10**, 197–209 (2009).
23. Cheng, G. *et al.* Self-Assembly of Smart Multifunctional Hybrid Compartments with Programmable Bioactivity. *Chem. Mater.* **29**, 2081–2089 (2017).
24. Nourian, Z., Roelofsen, W. & Danelon, C. Triggered Gene Expression in Fed-Vesicle Microreactors with a Multifunctional Membrane. *Angew. Chem. Int. Ed.* **51**, 3114–3118 (2012).
25. Chandrasekaran, A. R., Wady, H. & Subramanian, H. K. K. Nucleic Acid Nanostructures for Chemical and Biological Sensing. *Small* **12**, 2689–2700 (2016).
26. Krishnan, S. *et al.* Molecular transport through large-diameter DNA nanopores. *Nat.*

Commun. **7** (2016).

27. He, Y. *et al.* Hierarchical self-assembly of DNA into symmetric supramolecular polyhedra. *Nature* **452**, 198–201 (2008).
28. Rothemund, P. W. K. Folding DNA to create nanoscale shapes and patterns. *Nature* **440**, 297–302 (2006).
29. Dinsmore, A. D. *et al.* Colloidosomes: selectively permeable capsules composed of colloidal particles. *Science* **298**, 1006–1009 (2002).
30. Pickering, S. U. Emulsions. *J. Chem. Soc.* **91**, 2001–2021 (1907).
31. Cao, W., Huang, R. L., Qi, W., Su, R. X. & He, Z. M. Self-Assembly of Amphiphilic Janus Particles into Monolayer Capsules for Enhanced Enzyme Catalysis in Organic Media. *ACS Appl. Mater. Interfaces* **7**, 465–473 (2015).
32. Tang, J., Quinlan, P. J. & Tam, K. C. Stimuli-responsive Pickering emulsions: recent advances and potential applications. *Soft Matter* **11**, 3512–3529 (2015).
33. Kim, J.-W., Lee, D., Shum, H. C. & Weitz, D. A. Colloid Surfactants for Emulsion Stabilization. *Adv. Mater.* **20**, 3239–3243 (2008).
34. Shah, R. K., Kim, J. W. & Weitz, D. A. Monodisperse stimuli-responsive colloidosomes by self-assembly of microgels in droplets. *Langmuir* **26**, 1561–1565 (2010).
35. Binks, B. P. Particles as surfactants - similarities and differences. *Curr. Opin. Colloid Interface Sci.* **7**, 21–41 (2002).
36. Levine, S., Bowen, B. D. & Partridge, S. J. Stabilization of Emulsions by Fine Particles .1. Partitioning of Particles between Continuous Phase and Oil-Water Interface. *Colloids and Surfaces* **38**, 325–343 (1989).
37. Suzuki, Y., Endo, M., Yang, Y. Y. & Sugiyama, H. Dynamic assembly/disassembly processes of photoresponsive DNA origami nanostructures directly visualized on a lipid membrane surface. *J. Am. Chem. Soc.* **136**, 1714–1717 (2014).

38. Ruhland, T. M. *et al.* Influence of Janus particle shape on their interfacial behavior at liquid-liquid interfaces. *Langmuir* 29, 1388–1394 (2013).
39. List, J., Weber, M. & Simmel, F. C. Hydrophobic Actuation of a DNA Origami Bilayer Structure. *Angew. Chem. Int. Ed.* **53**, 4236–4239 (2014).
40. Dong, Y. C. *et al.* Cuboid Vesicles Formed by Frame-Guided Assembly on DNA Origami Scaffolds. *Angew. Chem. Int. Ed.* **56**, 1586–1589 (2017).
41. Guo, L. *et al.* Molecular diffusion measurement in lipid Bilayers over wide concentration ranges: A comparative study. *ChemPhysChem* **9**, 721–728 (2008).
42. Yanagisawa, M., Yoshida, T., Furuta, M., Nakata, S. & Tokita, M. Adhesive force between paired microdroplets coated with lipid monolayers. *Soft Matter* **9**, 5891–5897 (2013).
43. Kawano, R. *et al.* Automated Parallel Recordings of Topologically Identified Single Ion Channels. *Sci. Rep.* **3** (2013).
44. Ohara, M., Takinoue, M. & Kawano, R. Nanopore logic operation with DNA to RNA transcription in a droplet system. *ACS Synth. Biol.* **6**, 1427–1432 (2017).
45. Hille, B. *Ion Channels of Excitable Membranes*. 3rd ed. edn, (Sinauer Associate, 2001).
46. Castro, C. E., Su, H. J., Marras, A. E., Zhou, L. F. & Johnson, J. Mechanical design of DNA nanostructures. *Nanoscale* **7**, 5913–5921 (2015).
47. Takinoue, M., Kiga, D., Shohda, K. I. & Suyama, A. Experiments and simulation models of a basic computation element of an autonomous molecular computing system. *Phys. Rev. E* **78**, 041921 (2008).
48. Seelig, G., Soloveichik, D., Zhang, D. Y. & Winfree, E. Enzyme-free nucleic acid logic circuits. *Science* **314**, 1585–1588 (2006).
49. Douglas, S. M. *et al.* Rapid prototyping of 3D DNA-origami shapes with caDNAno. *Nucleic Acids Res.* **37**, 5001–5006 (2009).
50. Kitajima, T., Takinoue, M., Shohda, K. I. & Suyama, A. Design of code words for DNA

computers and nanostructures with consideration of hybridization kinetics. *DNA Comput.* **4848**, 119–129 (2008).